Acta Cryst E CRYSTALLOGRAPHIC COMMUNICATIONS

ISSN 2056-9890

(*E*)-1-(Benzo[*d*][1,3]dioxol-5-yl)-3-([2,2′-bithiophen]-5-yl)prop-2-en-1-one: crystal structure, UV–Vis analysis and theoretical studies of a new π-conjugated chalcone

Ainizatul Husna Anizaim, Muhamad Fikri Zaini, Muhammad Adlan Laruna, Ibrahim Abdul Razak and Suhana Arshad*

X-ray Crystallography Unit, School of Physics, Universiti Sains Malaysia, 11800 USM, Penang, Malaysia. *Correspondence e-mail: suhanaarshad@usm.my

Received 18 March 2019
Accepted 10 April 2019

Edited by J. Jasinsk, Keene State College, USA

Keywords: crystal structure; DFT; UV–Vis; HOMO–LUMO; Hirshfeld surface.

CCDC reference: 1899823

Supporting information: this article has supporting information at journals.iucr.org/e

In the title compound, $C_{18}H_{12}O_3S_2$, synthesized by the Claisen–Schmidt condensation method, the essentially planar chalcone unit adopts an *s-cis* configuration with respect to the carbonyl group within the ethylenic bridge. In the crystal, weak C—H···π interactions connect the molecules into zigzag chains along the *b*-axis direction. The molecular structure was optimized geometrically using Density Functional Theory (DFT) calculations at the B3LYP/6–311 G++(d,p) basis set level and compared with the experimental values. Molecular orbital calculations providing electron-density plots of HOMO and LUMO molecular orbitals and molecular electrostatic potentials (MEP) were also computed both with the DFT/B3LYP/6–311 G++(d,p) basis set. The experimental energy gap is 3.18 eV, whereas the theoretical HOMO–LUMO energy gap value is 2.73 eV. Hirshfeld surface analysis was used to further investigate the weak interactions present.

1. Chemical context

Chalcones are organic compounds composed of open-chain flavonoids in which the two aromatic rings are joined by a three-carbon α,β-unsaturated carbonyl system (Zingales *et al.*, 2016). Compounds with the chalcone backbone are becoming important in the design of new materials, employing donor–π–acceptor (*D*–π–*A*) bridge systems to further enhance their future development for optoelectronic applications. In principle, the intermolecular charge-transfer (ICT), HOMO–LUMO gap and optical properties can be tailored by attaching electron donors and acceptors of various electronic nature, assuring efficient *D*···*A* interactions and planarization of the entire molecule (Bureš, 2014). The presence of long π-conjugated systems in chalcones have been shown to turn them into chromophores whereby certain colours can be displayed as a result of absorbing light in the visible region (Asiri *et al.*, 2017). Electron-donating and accepting groups containing these chromophores have been examined for their applications in the field of material science. Additionally, the substitution of a phenyl group into a polythiophene compound stabilizes the conjugated π-bond system and forms a smaller band-gap material for supercapacitor applications (Mei-Rong *et al.*, 2014). As part of our ongoing studies utilizing thiophene-ring substituents with chalcone derivatives (Zainuri *et al.*, 2017), we hereby report the synthesis, structural, UV–Vis, Hirshfeld surface and DFT analyses of the title compound, (I).

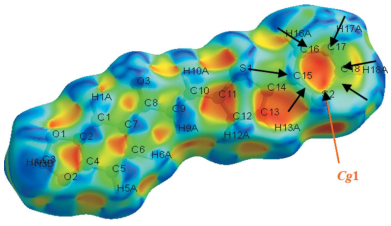

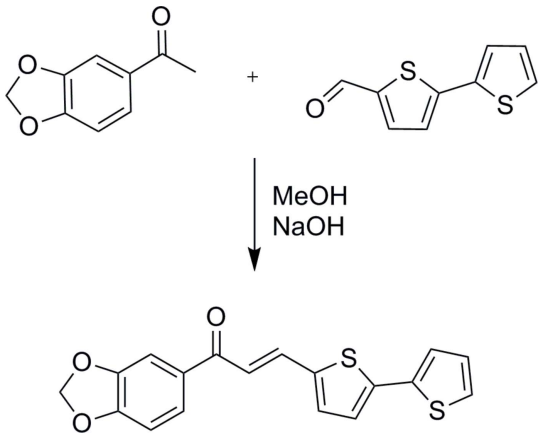

2. Structural commentary

The experimental and optimized structures of (I) are shown in Fig. 1*a* and 1*b*, respectively. The molecular structure consists of a 1,3-benzodioxole ring system (*A*; O1/O2/C1–C7) and two thiophene rings, *B* (S1/C11–C14) and *C* (S2/C15–C18), these substituent rings representing a donor–linker–acceptor conjugated system. Ring *A* [maximum deviation of 0.011 (4) Å at C3] forms dihedral angles of 1.88 (15) and 5.37 (16)°, respectively, with rings *B* [maximum deviations of 0.002 (3) and −0.002 (4) Å for C11 and C12, respectively] and *C* [maximum deviations of −0.009 (3) and 0.009 (3) Å for C15 and C16 respectively], respectively. The enone moiety [O3/C8–C10, maximum deviation of 0.014 (3) Å at C8] forms dihedral angles of 3.3 (2), 4.3 (2) and 7.4 (2)° with rings *A*, *B* and *C*, respectively. This planar conformation for the molecule indicates that the 1,3-benzodioxole group and the thiophene rings have stabilized the conjugated π-bond system.

The molecule adopts an *s-cis* configuration with respect to the C8═O3 [experimental = 1.229 (4) Å and DFT = 1.227 Å] bond length within the enone moiety (O3/C8–C10). The molecule is observed to be essentially planar (Fig. 1*c*) about the C9—C10 bond with a C8—C9—C10—C11 torsion angle of

Table 1
Hydrogen-bond geometry (Å, °).

Cg is the centroid of the S2/C15–C18 ring.

D—H···*A*	*D*—H	H···*A*	*D*···*A*	*D*—H···*A*
C3—H3*A*···*Cg*^{i}	0.97	2.74	3.472 (5)	132

Symmetry code: (i) $-x+1, y-\frac{1}{2}, -z+\frac{1}{2}$.

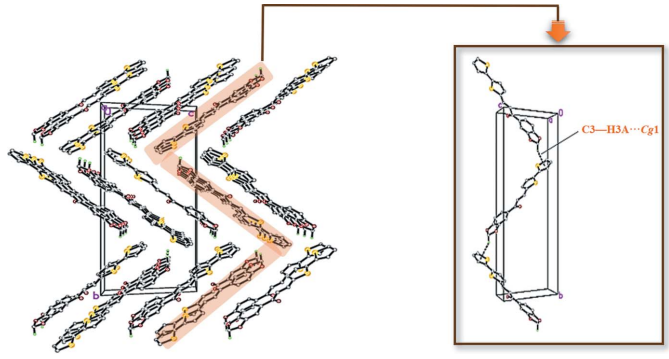

Figure 2
The crystal packing showing the C—H···π interactions (dashed lines).

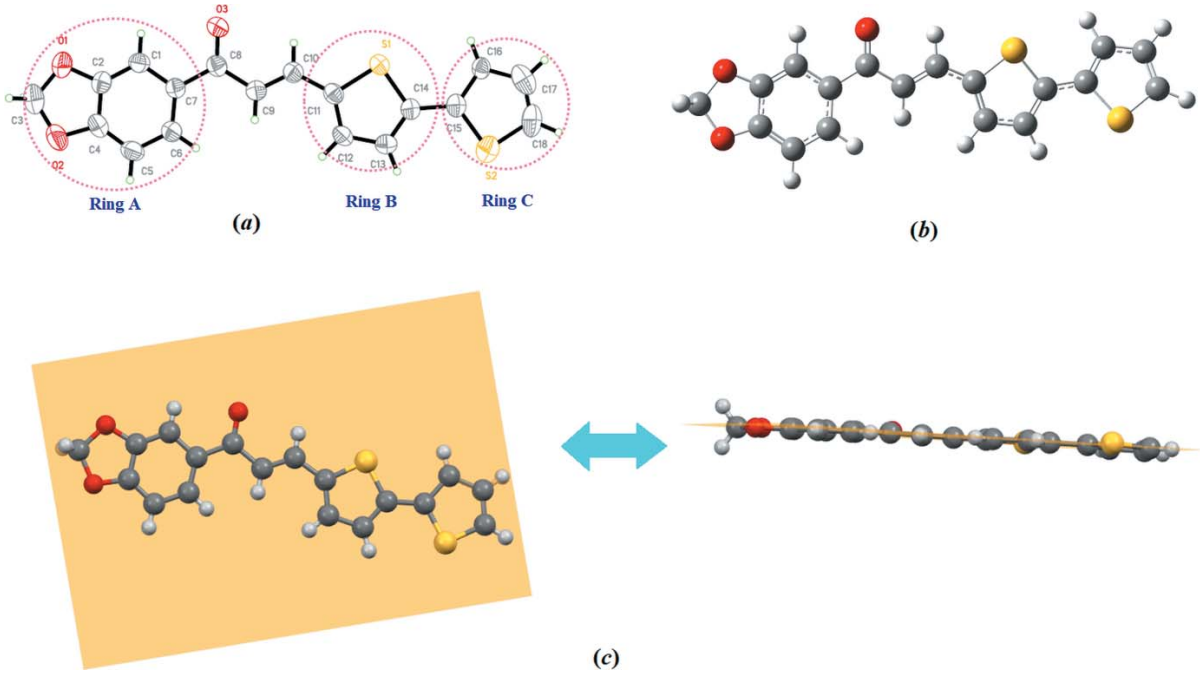

Figure 1
(*a*) Molecular structure of the title compound showing 50% probability displacement ellipsoids; (*b*) geometry-optimized molecular structure and (*c*) a representation of the molecule showing the planarity of all atoms.

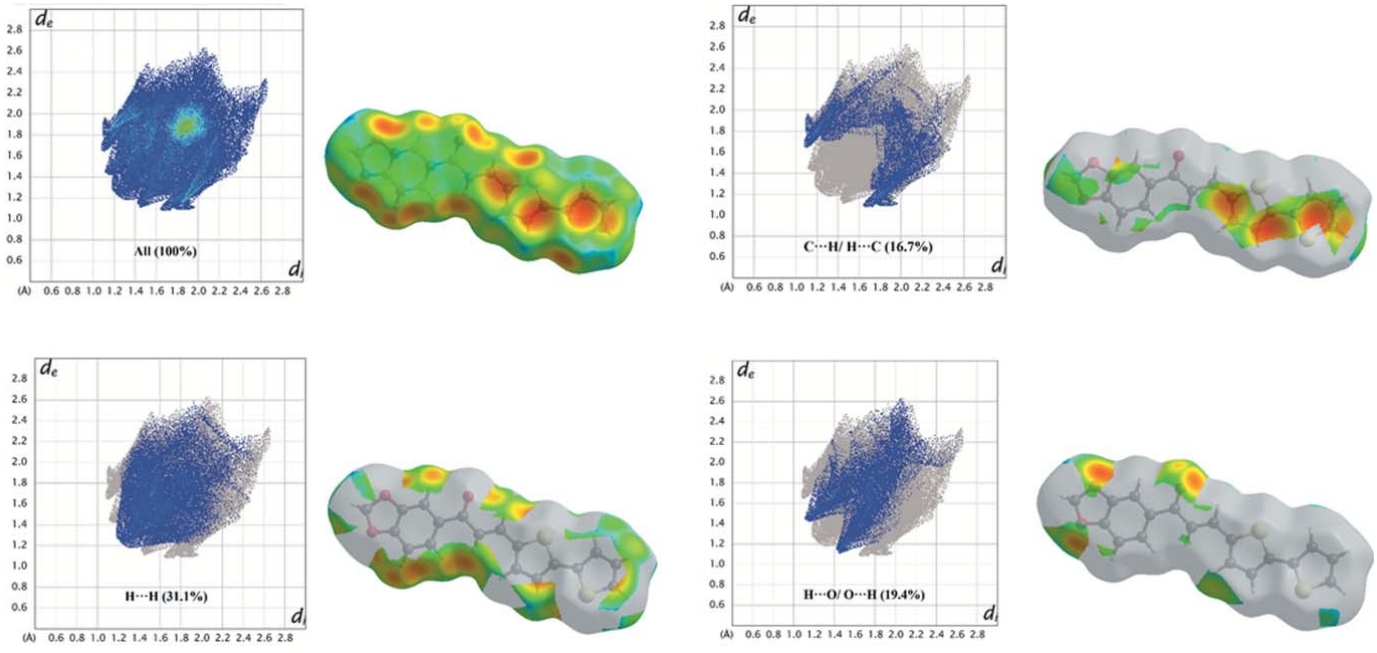

Figure 3
Two-dimensional fingerprint plots with a d_e view showing the percentage contributions of all interactions and the C···H/H···C, H···H and H···O/O···H interactions to the total Hirshfeld surface.

178.5 (3)°, whereas the corresponding DFT value is 179.6°. The slight difference is the result of the optimization being carried out in an isolated gaseous state whereas the experimental molecular structure could easily be affected by its normal environment (Zaini *et al.*, 2018).

For the theoretical geometry optimization calculation, the starting geometries of the compound were taken from the single-crystal X-ray refinement data. The optimization of the molecular geometries leading to energy minima was achieved using DFT [Becke's non-local three parameter exchange and Lee-Yang-Parr's correlation functional (B3LYP)] with the 6-311++G(d,p) basis set as implemented in the *Gaussian09W* software package (Frisch *et al.*, 2009). Selected bond lengths and angles for the experimental and theoretical (DFT) studies are compared in the supporting information; all values are within normal ranges (Allen *et al.*, 1987).

3. Supramolecular features

In the crystal, molecules are linked in a head-to-tail manner *via* C3—H3*A*···*Cg*($-x+1$, $y-\frac{1}{2}$, $-z+\frac{1}{2}$) interactions involving ring *C* (Table 1, Fig. 2), forming zigzag chains along the *b*-axis direction. In the absence of any classical hydrogen bonds, this interaction stabilizes the crystal structure. The chains stack along the *c*-axis direction.

4. Hirshfeld surface analysis

Hirshfeld surface analysis was undertaken using *Crystal Explorer 3.1* (Wolff *et al.*, 2012) to investigate the molecular packing. H···H interactions are the most important, contributing 31.1% to the overall crystal packing. In the fingerprint plot (Fig. 3) they are seen as widely scattered points of high density due to the large hydrogen-atom content of the molecule, with $d_e + d_i = 2.50$ Å (d_i and d_e are the distances to the nearest atom inside and outside the surface; Shit *et al.*, 2016). C···H/H···C contacts (16.7%) are indicated by a pair of peaks at $d_e + d_i = 2.75$ Å, while the H···O/O···H contacts (19.4%) are represented by a pair of short spikes at $d_e + d_i = 2.60$ Å. The significant contributions by H···H, H···C/C···H and H···O/O···H interactions suggest that weak hydrogen bonding and van der Waals interactions do play relevant roles in the crystal packing (Hathwar *et al.*, 2015). The surface mapped over shape-index reveals small changes in the surface shape, indicating the C—H···π (Fig. 4) interaction. The bright concave red spots in the region marked by arrows indicate atoms of the π-stacked molecule, whereas the convex blue

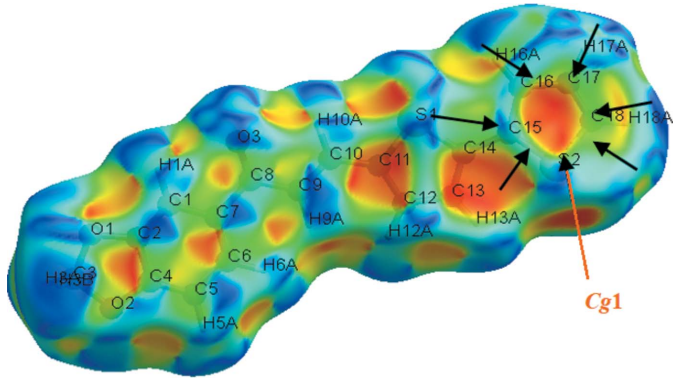

Figure 4
Hirshfeld surface mapped over shape-index.

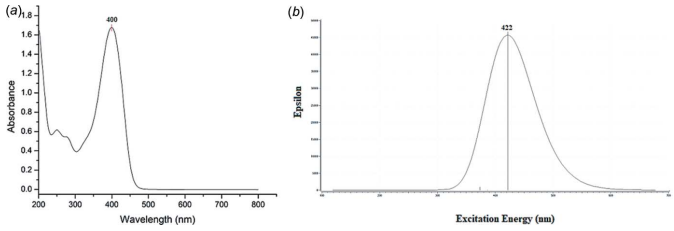

Figure 5
The (*a*) experimental and (*b*) calculated UV–Vis absorption spectra.

spots indicate ring atoms of the molecule inside the surface (Chkirate *et al.*, 2018).

5. UV–Vis and frontier molecular orbital analyses

The experimental UV–Vis absorption spectrum consists of one major band that lies in the visible region at 400 nm (Fig. 5*a*), while the simulated value is observed at 422 nm (Fig. 5*b*). The absorption maximum is assigned to the π–π^* transitions that arise from the carbonyl group (C═O) of the compound. The slight difference in wavelength is due to the fact that the experimental study is conducted in solution whereas the theoretical study is performed for a gaseous environment (Zainuri *et al.*, 2018*a*). The strong cut-off wavelength for the experimental study is 455 nm (Fig. 5*a*) with an energy band gap of 2.73 eV.

The highest occupied molecular orbital (HOMO) acts as an electron donor and represents the ability to donate electrons while the lowest unoccupied molecular orbital (LUMO) acts as the electron acceptor, representing the ability to accept electrons (Balasubramani *et al.*, 2018). The HOMO and LUMO electron-density plots were computed using the DFT/B3LYP/6-311 G++(d,p) basis set. The $E_{HOMO} - E_{LUMO}$ gap is calculated to be 3.18 eV. Generally, the value of the energy gap characterizes the chemical stability of the molecule

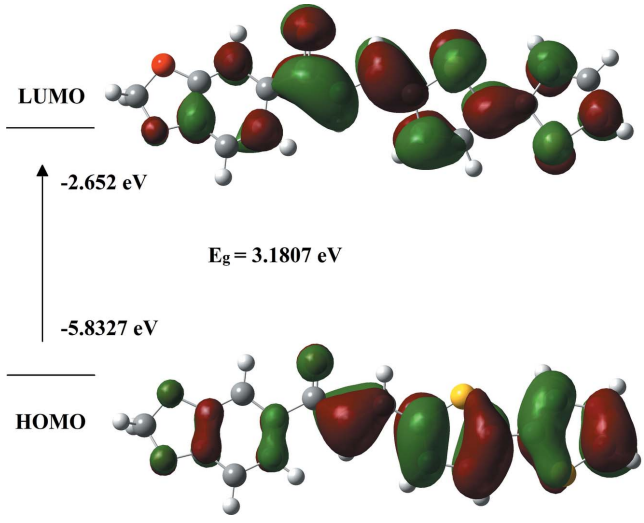

Figure 6
HOMO–LUMO molecular orbitals showing the ground to excited state electronic transitions.

(Zainuri *et al.*, 2018*b*). As shown in Fig. 6, the charge densities are accumulated over the entire molecule for the HOMO and LUMO states. A large HOMO–LUMO energy gap defines it as a 'hard' molecule while a small one defines a 'soft' molecule (Bayar *et al.*, 2018). Hard molecules are less polarizable than the soft ones as there is a need of higher energy for excitation (Balasubramani *et al.*, 2018). The energy gap value in the title compound indicates good stability and a high chemical hardness.

6. Molecular electrostatic potentials

Molecular electrostatic potentials (MEP) are useful in investigating the relationship between the molecular structure and its physicochemical properties, visualizing the molecular size and shape, along with the charge distributions in molecules in terms of colour grading (Zainuri *et al.*, 2018*b*). The MEP map (Fig. 7) was calculated at the B3LYP/6-311G++ (d,p) level of theory. The red- and blue-coloured regions indicate nucleophiles that are electron rich, and electrophile regions that are electron poor, respectively. The remaining white regions indicate neutral atoms. Information about intermolecular interactions within the compound can be obtained from these regions (Gunasekaran *et al.*, 2008). In the title molecule, the reactive site, localized in the carbonyl group, is shown in red. It possesses the most negative potential and is thus the strongest repulsion site (electrophilic attack). The blue spots indicate the strongest attraction regions, which are occupied mostly by hydrogen atoms (Zaini *et al.*, 2019).

7. Database survey

A search of the Cambridge Structural Database (Version 5.39, last update November 2017; Groom *et al.*, 2016) revealed four thiophene-substituted compounds with a different ketone on the chalcone: (*E*)-1-(2-aminophenyl)-3-(thiophen-2-yl)prop-2-en-1-one (Chantrapromma *et al.*, 2013), (2*E*)-3-(5-bromo-2-thienyl)-1-(4-hydroxyphenyl)prop-2-en-1-one (Narayana *et al.*, 2007), 1-(4-bromophenyl)-3-(2-thienyl)prop-2-en-1-one (Patil *et al.*, 2006) and (2*E*)-1-(4-bromophenyl)-3-(thiophen-2-yl)prop-2-en-1-one (Arshad *et al.*, 2017). Other related compounds that have a similar benzo[*d*]dioxol substituent on the chalcone are (2*E*)-1-(1,3-benzodioxol-5-yl)-3-(4-chlorophenyl)prop-2-en-1-one (Sreevidya *et al.*, 2010) and (*E*)-1-

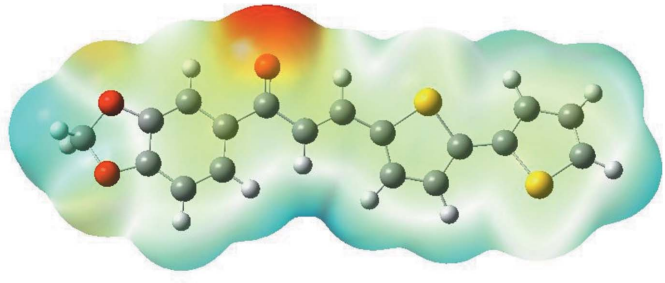

Figure 7
Theoretical molecular electrostatic potential surface calculated at the DFT/B3LYP/6–311G++ (d,p) basis set level.

Table 2
Experimental details.

Crystal data	
Chemical formula	$C_{18}H_{12}O_3S_2$
M_r	340.40
Crystal system, space group	Monoclinic, $P2_1/c$
Temperature (K)	296
a, b, c (Å)	6.030 (1), 24.875 (5), 11.239 (2)
β (°)	114.249 (2)
V (Å^3)	1537.1 (5)
Z	4
Radiation type	Mo $K\alpha$
μ (mm^{-1})	0.36
Crystal size (mm)	0.19 × 0.15 × 0.06
Data collection	
Diffractometer	Bruker APEXII CCD
Absorption correction	Multi-scan (*SADABS*; Bruker, 2009)
T_{min}, T_{max}	0.875, 0.924
No. of measured, independent and observed [$I > 2\sigma(I)$] reflections	30820, 3024, 2096
R_{int}	0.078
(sin $\theta/\lambda)_{max}$ (Å^{-1})	0.617
Refinement	
$R[F^2 > 2\sigma(F^2)]$, $wR(F^2)$, S	0.058, 0.164, 1.04
No. of reflections	3024
No. of parameters	208
H-atom treatment	H-atom parameters constrained
$\Delta\rho_{max}$, $\Delta\rho_{min}$ (e Å^{-3})	0.41, −0.47

Computer programs: *APEX2* and *SAINT* (Bruker, 2009), *SHELXS97* (Sheldrick, 2008), *SHELXL2014* (Sheldrick, 2015) and *SHELXTL* (Sheldrick, 2008).

(1,3-benzodioxol-5-yl)-3-(3-bromophenyl)prop-2-en-1-one (Li *et al.*, 2008).

In terms of intermolecular interactions, (*E*)-1-(2-aminophenyl)-3-(thiophen-2-yl)prop-2-en-1-one (Chantrapromma *et al.*, 2013) exhibits a strong intermolecular C—H···O interaction by which two adjacent molecules are linked in an antiparallel face-to-face manner into chains along the *c*-axis direction. Meanwhile, a weak intermolecular O—H···O interaction is observed in (2*E*)-3-(5-bromo-2-thienyl)-1-(4-hydroxyphenyl)prop-2-en-1-one (Narayana *et al.*, 2007). Similar to the situation in (I), weak intermolecular C—H···π interactions link the molecules of 1-(4-bromophenyl)-3-(2-thienyl)prop-2-en-1-one (Patil *et al.*, 2006) into chains along the *b*-axis direction. Lastly, an intermolecular C—H···Cl interaction, involving the terminal chloro-substituted phenyl ring, is also found in (2*E*)-1-(1,3-benzodioxol-5-yl)-3-(4-chlorophenyl)prop-2-en-1-one (Sreevidya *et al.*, 2010).

8. Synthesis and crystallization

A mixture of 3′,4′-(methylenedioxy)acetophenone (0.5 mmol) and 2,2′-bithiophene-5-carboxaldehyde (0.5 mmol) was dissolved in methanol. A catalytic amount of NaOH was added dropwise with vigorous stirring. The reaction mixture was stirred for about 5 h at room temperature and then poured into ice-cold water. The resulting crude solid was collected by filtration. Single crystals were grown from an acetone solution by slow evaporation.

9. Refinement

Crystal data collection and structure refinement details are summarized in Table 2. All H atoms were positioned geometrically (C—H = 0.93 and 0.97 Å) and refined using a riding model with U_{iso}(H) = 1.2 U_{eq}(C). One outlier (104) was omitted from the final refinement.

Funding information

The authors would like to thank the Malaysian Government and Universiti Sains Malaysia (USM) for providing facilities and funding to conduct this work under the Fundamental Research Grant Scheme (FGRS) No. 203.PFIZIK.6711606.

References

Allen, F. H., Kennard, O., Watson, D. G., Brammer, L., Orpen, A. G. & Taylor, R. (1987). *J. Chem. Soc. Perkin Trans. 2*, pp. S1–S19.
Arshad, M. N., Al-Dies, A. M., Asiri, A. M., Khalid, M., Birinji, A. S., Al-Amry, K. A. & Braga, A. A. C. (2017). *J. Mol. Struct.* **1141**, 142–156.
Asiri, M., Sobahi, T. R., Osman, O. I. & Khan, S. A. (2017). *J. Mol. Struct.* **1128**, 636–644.
Balasubramani, K., Premkumar, G., Sivajeyanthi, P., Jeevaraj, M., Edison, B. & Swu, T. (2018). *Acta Cryst.* E**74**, 1500–1503.
Bayar, I., Khedhiri, L., Soudani, S., Lefebvre, F., Pereira da Silva, P. S. & Ben Nasr, C. (2018). *J. Mol. Struct.* **1161**, 185–193.
Bruker (2009). *APEX2*, *SAINT* and *SADABS*. Bruker AXS Inc., Madison, Wisconsin, USA.
Bureš, F. (2014). *RSC Adv.* **4**, 58826–58851.
Chantrapromma, S., Ruanwas, P., Boonnak, N. & Fun, H.-K. (2013). *Acta Cryst.* E**69**, o1004–o1005.
Chkirate, K., Sebbar, N. K., Hökelek, T., Krishnan, D., Mague, J. T. & Essassi, E. M. (2018). *Acta Cryst.* E**74**, 1669–1673.
Frisch, M. J., Trucks, G. W., Schlegel, H. B., Scuseria, G. E., Robb, M. A., Cheeseman, J. R., Scalmani, G., Barone, V., Mennucci, B., Petersson, G. A., Nakatsuji, H., Caricato, M., Li, X., Hratchian, H. P., Izmaylov, A. F., Bloino, J., Zheng, G., Sonnenberg, J. L., Hada, M., Ehara, M., Toyota, K., Fukuda, R., Hasegawa, J., Ishida, M., Nakajima, T., Honda, Y., Kitao, O., Nakai, H., Vreven, T., Montgomery, J. A. Jr, Peralta, J. E., Ogliaro, F., Bearpark, M., Heyd, J. J., Brothers, E., Kudin, K. N., Staroverov, V. N., Keith, T., Kobayashi, R., Normand, J., Raghavachari, K., Rendell, A., Burant, J. C., Iyengar, S. S., Tomasi, J., Cossi, M., Rega, N., Millam, J. M., Klene, M., Knox, J. E., Cross, J. B., Bakken, V., Adamo, C., Jaramillo, J., Gomperts, R., Stratmann, R. E., Yazyev, O., Austin, A. J., Cammi, R., Pomelli, C., Ochterski, J. W., Martin, R. L., Morokuma, K., Zakrzewski, V. G., Voth, G. A., Salvador, P., Dannenberg, J. J., Dapprich, S., Daniels, A. D., Farkas, Ö., Foresman, J. B., Ortiz, J. V., Cioslowski, J. & Fox, D. J. (2009). *Gaussian 09*, Revision A1. Gaussian, Inc., Wallingford CT, USA.
Groom, C. R., Bruno, I. J., Lightfoot, M. P. & Ward, S. C. (2016). *Acta Cryst.* B**72**, 171–179.
Gunasekaran, S., Kumaresan, S., Arunbalaji, R., Anand, G. & Srinivasan, S. (2008). *J. Chem. Sci.* **120**, 780–785.
Hathwar, V. R., Sist, M., Jørgensen, M. R. V., Mamakhel, A. H., Wang, X., Hoffmann, C. M., Sugimoto, K., Overgaard, J. & Iversen, B. B. (2015). *IUCrJ*, **2**, 563–574.
Li, H., Sreevidya, T. V., Narayana, B., Sarojini, B. K. & Yathirajan, H. S. (2008). *Acta Cryst.* E**64**, o2387.
Mei-Rong, Y., Yu, S. & Yong-Jin, X. (2014). *SpringerPlus*, **3**, 701–714.
Narayana, B., Lakshmana, K., Sarojini, B. K., Yathirajan, H. S. & Bolte, M. (2007). *Acta Cryst.* E**63**, o4552.
Patil, P. S., Ng, S.-L., Razak, I. A., Fun, H.-K. & Dharmaprakash, S. M. (2006). *Acta Cryst.* E**62**, o3718–o3720.
Sheldrick, G. M. (2008). *Acta Cryst.* A**64**, 112–122.

Sheldrick, G. M. (2015). *Acta Cryst.* C**71**, 3–8.
Shit, S., Marschner, C. & Mitra, S. (2016). *Acta Chim. Slov*. **63**, 129–137.
Sreevidya, T. V., Narayana, B. & Yathirajan, H. S. (2010). *Cent. Eur. J. Chem.* **8**, 174–181.
Wolff, S. K., Grimwood, D. J., McKinnon, J. J., Turner, M. J., Jayatilaka, D. & Spackman, M. A. (2012). *Crystal Explorer.* University of Western Australia, Perth.
Zaini, M. F., Razak, I. A., Khairul, W. M. & Arshad, S. (2018). *Acta Cryst.* E**74**, 1589–1594.
Zaini, M. F., Razak, I. A., Anis, M. Z. & Arshad, S. (2019). *Acta Cryst.* E**75**, 58–63.
Zainuri, D. A., Arshad, S., Khalib, N. C. & Razak, I. A. (2017). *Mol. Cryst. Liq. Cryst.* **650**, 87–101.
Zainuri, D. A., Razak, I. A. & Arshad, S. (2018*a*). *Acta Cryst.* E**74**, 1427–1432.
Zainuri, D. A., Razak, I. A. & Arshad, S. (2018*b*). *Acta Cryst.* E**74**, 1491–1496.
Zingales, S. K., Moore, M. E., Goetz, A. D. & Padgett, C. W. (2016). *Acta Cryst.* E**72**, 955–958.

supporting information

Acta Cryst. (2019). E**75**, 632-637 [https://doi.org/10.1107/S2056989019004912]

(*E*)-1-(Benzo[*d*][1,3]dioxol-5-yl)-3-([2,2′-bithiophen]-5-yl)prop-2-en-1-one: crystal structure, UV–Vis analysis and theoretical studies of a new π-conjugated chalcone

Ainizatul Husna Anizaim, Muhamad Fikri Zaini, Muhammad Adlan Laruna, Ibrahim Abdul Razak and Suhana Arshad

Computing details

Data collection: *APEX2* (Bruker, 2009); cell refinement: *SAINT* (Bruker, 2009); data reduction: *SAINT* (Bruker, 2009); program(s) used to solve structure: *SHELXS97* (Sheldrick, 2008); program(s) used to refine structure: *SHELXL2014* (Sheldrick, 2015); molecular graphics: *SHELXTL* (Sheldrick, 2008); software used to prepare material for publication: *SHELXTL* (Sheldrick, 2008).

(*E*)-1-(Benzo[*d*][1,3]dioxol-5-yl)-3-([2,2′-bithiophen]-5-yl)prop-2-en-1-one

Crystal data

$C_{18}H_{12}O_3S_2$
M_r = 340.40
Monoclinic, $P2_1/c$
a = 6.030 (1) Å
b = 24.875 (5) Å
c = 11.239 (2) Å
β = 114.249 (2)°
V = 1537.1 (5) Å^3
Z = 4
$F(000)$ = 704
D_x = 1.471 Mg m^{-3}
Mo $K\alpha$ radiation, λ = 0.71073 Å
Cell parameters from 3229 reflections
θ = 2.6–19.6°
μ = 0.36 mm^{-1}
T = 296 K
Plate, yellow
0.19 × 0.15 × 0.06 mm

Data collection

Bruker APEXII CCD diffractometer
φ and ω scans
Absorption correction: multi-scan (SADABS; Bruker, 2009)
T_{min} = 0.875, T_{max} = 0.924
30820 measured reflections
3024 independent reflections
2096 reflections with $I > 2\sigma(I)$
R_{int} = 0.078
θ_{max} = 26.0°, θ_{min} = 2.2°
h = −7→7
k = −30→30
l = −13→13

Refinement

Refinement on F^2
Least-squares matrix: full
$R[F^2 > 2\sigma(F^2)]$ = 0.058
$wR(F^2)$ = 0.164
S = 1.04
3024 reflections
208 parameters
0 restraints
Hydrogen site location: inferred from neighbouring sites
H-atom parameters constrained

$w = 1/[\sigma^2(F_o^2) + (0.074P)^2 + 1.2156P]$
where $P = (F_o^2 + 2F_c^2)/3$
$(\Delta/\sigma)_{max} < 0.001$

$\Delta\rho_{max} = 0.41$ e Å^{-3}
$\Delta\rho_{min} = -0.47$ e Å^{-3}

Special details

Experimental. The following wavelength and cell were deduced by SADABS from the direction cosines etc. They are given here for emergency use only: CELL 0.71075 11.261 24.951 12.083 90.028 114.196 90.000

Geometry. All esds (except the esd in the dihedral angle between two l.s. planes) are estimated using the full covariance matrix. The cell esds are taken into account individually in the estimation of esds in distances, angles and torsion angles; correlations between esds in cell parameters are only used when they are defined by crystal symmetry. An approximate (isotropic) treatment of cell esds is used for estimating esds involving l.s. planes.

Fractional atomic coordinates and isotropic or equivalent isotropic displacement parameters (Å²)

	x	*y*	*z*	U_{iso}*/U_{eq}
S1	0.28791 (16)	0.61675 (4)	−0.12250 (9)	0.0500 (3)
S2	0.7476 (2)	0.71610 (5)	−0.24635 (12)	0.0759 (4)
O1	0.3608 (5)	0.35799 (12)	0.5854 (3)	0.0715 (8)
O2	0.7813 (5)	0.35937 (12)	0.6897 (3)	0.0693 (8)
O3	0.1080 (4)	0.48699 (11)	0.1984 (3)	0.0628 (8)
C1	0.3315 (6)	0.42199 (14)	0.4126 (3)	0.0458 (8)
H1A	0.1626	0.4211	0.3711	0.055*
C2	0.4540 (6)	0.39239 (14)	0.5213 (3)	0.0468 (8)
C3	0.5656 (8)	0.33666 (17)	0.6914 (4)	0.0681 (11)
H3A	0.5690	0.2979	0.6837	0.082*
H3B	0.5551	0.3452	0.7731	0.082*
C4	0.7034 (7)	0.39318 (14)	0.5843 (3)	0.0495 (9)
C5	0.8413 (6)	0.42354 (15)	0.5408 (4)	0.0549 (9)
H5A	1.0100	0.4239	0.5838	0.066*
C6	0.7201 (6)	0.45425 (14)	0.4288 (3)	0.0478 (8)
H6A	0.8102	0.4754	0.3965	0.057*
C7	0.4692 (6)	0.45409 (13)	0.3647 (3)	0.0388 (7)
C8	0.3316 (6)	0.48707 (13)	0.2464 (3)	0.0439 (8)
C9	0.4651 (6)	0.52000 (14)	0.1886 (3)	0.0472 (8)
H9A	0.6341	0.5210	0.2290	0.057*
C10	0.3511 (6)	0.54804 (13)	0.0810 (3)	0.0443 (8)
H10A	0.1824	0.5455	0.0418	0.053*
C11	0.4651 (6)	0.58250 (13)	0.0185 (3)	0.0420 (8)
C12	0.7044 (6)	0.59448 (15)	0.0536 (3)	0.0502 (9)
H12A	0.8296	0.5800	0.1266	0.060*
C13	0.7433 (6)	0.63090 (15)	−0.0313 (4)	0.0514 (9)
H13A	0.8971	0.6429	−0.0195	0.062*
C14	0.5365 (6)	0.64701 (13)	−0.1323 (3)	0.0406 (8)
C15	0.5055 (6)	0.68374 (13)	−0.2391 (3)	0.0440 (8)
C16	0.2850 (6)	0.69828 (13)	−0.3490 (3)	0.0414 (8)
H16A	0.1299	0.6861	−0.3641	0.050*
C17	0.3416 (9)	0.73361 (17)	−0.4296 (4)	0.0707 (12)
H17A	0.2237	0.7470	−0.5069	0.085*
C18	0.5754 (9)	0.74663 (17)	−0.3879 (4)	0.0745 (13)

H18A	0.6365	0.7699	−0.4319	0.089*

Atomic displacement parameters (Å²)

	U^{11}	U^{22}	U^{33}	U^{12}	U^{13}	U^{23}
S1	0.0423 (5)	0.0579 (6)	0.0427 (5)	−0.0005 (4)	0.0104 (4)	0.0114 (4)
S2	0.0742 (8)	0.0772 (8)	0.0827 (9)	−0.0029 (6)	0.0389 (7)	0.0186 (6)
O1	0.0704 (18)	0.0748 (19)	0.0736 (19)	0.0013 (15)	0.0338 (16)	0.0314 (16)
O2	0.0705 (18)	0.0690 (19)	0.0551 (17)	0.0058 (15)	0.0124 (14)	0.0231 (14)
O3	0.0410 (14)	0.0757 (19)	0.0598 (17)	−0.0031 (12)	0.0086 (12)	0.0221 (14)
C1	0.0394 (18)	0.050 (2)	0.046 (2)	0.0012 (15)	0.0160 (15)	0.0002 (16)
C2	0.053 (2)	0.043 (2)	0.048 (2)	−0.0008 (16)	0.0243 (17)	0.0030 (16)
C3	0.094 (3)	0.057 (3)	0.054 (2)	0.003 (2)	0.031 (2)	0.011 (2)
C4	0.058 (2)	0.044 (2)	0.0394 (19)	0.0029 (17)	0.0126 (17)	0.0026 (15)
C5	0.0418 (19)	0.058 (2)	0.053 (2)	−0.0009 (17)	0.0081 (17)	0.0032 (19)
C6	0.0446 (19)	0.049 (2)	0.046 (2)	−0.0024 (15)	0.0139 (16)	0.0039 (16)
C7	0.0427 (17)	0.0354 (17)	0.0361 (17)	−0.0030 (14)	0.0139 (14)	−0.0039 (14)
C8	0.0471 (19)	0.0412 (19)	0.0389 (18)	−0.0015 (15)	0.0131 (15)	−0.0026 (15)
C9	0.0430 (18)	0.049 (2)	0.046 (2)	−0.0044 (15)	0.0148 (16)	0.0025 (17)
C10	0.0440 (18)	0.0462 (19)	0.0408 (19)	−0.0014 (15)	0.0155 (15)	0.0005 (16)
C11	0.0443 (18)	0.0437 (19)	0.0364 (18)	0.0052 (14)	0.0152 (15)	0.0000 (15)
C12	0.0418 (19)	0.061 (2)	0.042 (2)	0.0075 (16)	0.0112 (15)	0.0116 (17)
C13	0.0394 (18)	0.059 (2)	0.055 (2)	0.0030 (16)	0.0191 (17)	0.0067 (18)
C14	0.0456 (18)	0.0368 (18)	0.0411 (18)	0.0019 (14)	0.0196 (15)	−0.0016 (14)
C15	0.056 (2)	0.0369 (18)	0.0430 (19)	0.0032 (15)	0.0236 (16)	−0.0011 (15)
C16	0.0505 (19)	0.0413 (19)	0.0311 (17)	−0.0042 (15)	0.0155 (15)	0.0005 (14)
C17	0.091 (3)	0.067 (3)	0.048 (2)	0.024 (2)	0.021 (2)	0.006 (2)
C18	0.115 (4)	0.059 (3)	0.066 (3)	0.004 (3)	0.055 (3)	0.014 (2)

Geometric parameters (Å, º)

S1—C14	1.720 (3)	C6—H6A	0.9300
S1—C11	1.728 (3)	C7—C8	1.491 (4)
S2—C18	1.682 (4)	C8—C9	1.473 (5)
S2—C15	1.698 (3)	C9—C10	1.318 (5)
O1—C2	1.378 (4)	C9—H9A	0.9300
O1—C3	1.420 (5)	C10—C11	1.448 (4)
O2—C4	1.369 (4)	C10—H10A	0.9300
O2—C3	1.425 (5)	C11—C12	1.364 (5)
O3—C8	1.229 (4)	C12—C13	1.404 (5)
C1—C2	1.356 (5)	C12—H12A	0.9300
C1—C7	1.409 (5)	C13—C14	1.357 (5)
C1—H1A	0.9300	C13—H13A	0.9300
C2—C4	1.375 (5)	C14—C15	1.458 (5)
C3—H3A	0.9700	C15—C16	1.441 (5)
C3—H3B	0.9700	C16—C17	1.401 (5)
C4—C5	1.355 (5)	C16—H16A	0.9300
C5—C6	1.395 (5)	C17—C18	1.330 (6)

C5—H5A	0.9300	C17—H17A	0.9300
C6—C7	1.383 (4)	C18—H18A	0.9300

C14—S1—C11	92.72 (16)	C10—C9—C8	121.6 (3)
C18—S2—C15	92.9 (2)	C10—C9—H9A	119.2
C2—O1—C3	105.6 (3)	C8—C9—H9A	119.2
C4—O2—C3	105.3 (3)	C9—C10—C11	125.8 (3)
C2—C1—C7	117.6 (3)	C9—C10—H10A	117.1
C2—C1—H1A	121.2	C11—C10—H10A	117.1
C7—C1—H1A	121.2	C12—C11—C10	130.2 (3)
C1—C2—C4	122.1 (3)	C12—C11—S1	109.9 (3)
C1—C2—O1	128.3 (3)	C10—C11—S1	119.9 (2)
C4—C2—O1	109.6 (3)	C11—C12—C13	113.4 (3)
O1—C3—O2	109.0 (3)	C11—C12—H12A	123.3
O1—C3—H3A	109.9	C13—C12—H12A	123.3
O2—C3—H3A	109.9	C14—C13—C12	113.9 (3)
O1—C3—H3B	109.9	C14—C13—H13A	123.0
O2—C3—H3B	109.9	C12—C13—H13A	123.0
H3A—C3—H3B	108.3	C13—C14—C15	129.5 (3)
C5—C4—O2	127.7 (3)	C13—C14—S1	110.1 (3)
C5—C4—C2	121.7 (3)	C15—C14—S1	120.4 (3)
O2—C4—C2	110.5 (3)	C16—C15—C14	128.6 (3)
C4—C5—C6	117.3 (3)	C16—C15—S2	110.4 (2)
C4—C5—H5A	121.3	C14—C15—S2	121.0 (3)
C6—C5—H5A	121.3	C17—C16—C15	109.2 (3)
C7—C6—C5	121.6 (3)	C17—C16—H16A	125.4
C7—C6—H6A	119.2	C15—C16—H16A	125.4
C5—C6—H6A	119.2	C18—C17—C16	115.4 (4)
C6—C7—C1	119.6 (3)	C18—C17—H17A	122.3
C6—C7—C8	123.5 (3)	C16—C17—H17A	122.3
C1—C7—C8	116.9 (3)	C17—C18—S2	112.1 (3)
O3—C8—C9	120.5 (3)	C17—C18—H18A	123.9
O3—C8—C7	119.9 (3)	S2—C18—H18A	123.9
C9—C8—C7	119.6 (3)		

C7—C1—C2—C4	0.2 (5)	C7—C8—C9—C10	177.2 (3)
C7—C1—C2—O1	−179.5 (3)	C8—C9—C10—C11	178.5 (3)
C3—O1—C2—C1	179.0 (4)	C9—C10—C11—C12	−0.8 (6)
C3—O1—C2—C4	−0.6 (4)	C9—C10—C11—S1	−179.8 (3)
C2—O1—C3—O2	0.5 (4)	C14—S1—C11—C12	−0.3 (3)
C4—O2—C3—O1	−0.2 (4)	C14—S1—C11—C10	178.8 (3)
C3—O2—C4—C5	−179.0 (4)	C10—C11—C12—C13	−178.6 (3)
C3—O2—C4—C2	−0.2 (4)	S1—C11—C12—C13	0.4 (4)
C1—C2—C4—C5	−0.2 (6)	C11—C12—C13—C14	−0.3 (5)
O1—C2—C4—C5	179.5 (3)	C12—C13—C14—C15	−179.5 (3)
C1—C2—C4—O2	−179.2 (3)	C12—C13—C14—S1	0.1 (4)
O1—C2—C4—O2	0.5 (4)	C11—S1—C14—C13	0.1 (3)
O2—C4—C5—C6	178.7 (3)	C11—S1—C14—C15	179.8 (3)

C2—C4—C5—C6	0.0 (6)	C13—C14—C15—C16	176.6 (3)
C4—C5—C6—C7	0.3 (6)	S1—C14—C15—C16	−3.0 (5)
C5—C6—C7—C1	−0.4 (5)	C13—C14—C15—S2	−3.2 (5)
C5—C6—C7—C8	178.7 (3)	S1—C14—C15—S2	177.20 (19)
C2—C1—C7—C6	0.1 (5)	C18—S2—C15—C16	−1.2 (3)
C2—C1—C7—C8	−179.0 (3)	C18—S2—C15—C14	178.6 (3)
C6—C7—C8—O3	−176.3 (3)	C14—C15—C16—C17	−178.2 (3)
C1—C7—C8—O3	2.9 (5)	S2—C15—C16—C17	1.6 (4)
C6—C7—C8—C9	3.1 (5)	C15—C16—C17—C18	−1.4 (5)
C1—C7—C8—C9	−177.8 (3)	C16—C17—C18—S2	0.5 (5)
O3—C8—C9—C10	−3.5 (5)	C15—S2—C18—C17	0.4 (4)

Hydrogen-bond geometry (Å, º)

Cg is the centroid of the S2/C15–C18 ring.

D—H···*A*	*D*—H	H···*A*	*D*···*A*	*D*—H···*A*
C3—H3*A*···*Cg*^{i}	0.97	2.74	3.472 (5)	132

Symmetry code: (i) −*x*+1, *y*−1/2, −*z*+1/2.